Journal of Computational Physics **148,** 322–340 (1999)
Article ID jcph.1998.6112, available online at http://www.idealibrary.com on IDEAL®

A Large-Eddy Simulation Methodology in Generalized Curvilinear Coordinates

Stephen. A. Jordan

Naval Undersea Warfare Center, Code 8322, Building 1246, Newport, Rhode Island 02841
E-mail: jordan@code 83.npt.nuwc.navy.mil

Received December 3, 1996; revised July 30, 1998

A generalized curvilinear coordinate formulation for the large-eddy simulation (LES) that centers on the fact that two spatial operations are necessary to complete the derivation is proposed. The recommended order of operations is to transform the full resolution system prior to filtering. This sequence rationally directs the filter operation along the curvilinear lines, thereby facilitating explicit evaluation of the Leonard stress and its isolation from the relative errors associated with the finite-difference approximations of the convective derivative. Representing the transformation metrics as filtered quantities in the formulation is justified through their numerical approximation. The generalized LES formulation was tested using direct numerical simulation results of the circular cylinder near wake at $\mathrm{Re} = 3400$. No discernible differences were detected in the spectral energies of the turbulent fluctuations by filtering in either the physical domain or the transformed space. However, the latter filtering scheme was considerably cheaper. In the transformed space, high-order numerical approximations are required for the convective derivatives to inhibit overshadowing of the concurrent contributions by the Leonard stress at all wavenumbers.

I. INTRODUCTION

The recent gain in popularity of the large-eddy simulation (LES) as a useful computational fluid dynamics (CFD) approach to understanding turbulence rests principally on the rapid advancements in supercomputer technology, as well as the encouraging developments in the methodology itself. The LES philosophy is founded on resolving (computing) the large-scale energy-dominate structures of the turbulent motion while modeling only the remaining fine-scale eddies which tend toward homogeneous and isotropic characteristics. Demarcation between the resolved and modeled turbulent scales is formally instituted by spatially filtering the Navier–Stokes equations. In many finite-difference computations, however, this filter is actually implemented implicitly through the grid's resolution. The local filter width in these simulations is equivalent to the local grid spacing. Those length scales lying beneath the

0021-9991/99 $30.00

grid's resolution comprise the subgrid scales (SGS) of the turbulent field. To close the LES formulation, a representative model is designed for the SGS field which usually embodies most of the equilibrium range of the turbulent spectral energy.

Historically, most LES applications possess a certain commonality in that the respective topologies are geometrically simple. A few notable exceptions include Schumann and Krettenauer [1], who simulated turbulent convection over a sinusoidal undulated terrain at an infinite Rayleigh number, and Lund and Moin [2] (as well as Breuer and Rodi [3]), who resolved the Reynolds stress statistics in the spatially evolving boundary layers along the upper and lower walls of a concave-surface channel. In addition, a thorough numerical study of the cylinder wake using a compressible flow form of the LES equations was completed by Beaudan and Moin [4] at a moderate Reynolds number of 3900, based on the cylinder diameter. Although these exceptions required coordinate transformation of the basic Cartesian form of the governing LES equations to accommodate a boundary-fitted grid to the wall curvature, no formal treatment of the transformation operation nor the accompanying metrics was addressed.

The present work aims to formally document a fundamental generalized curvilinear coordinate formulation of the LES equations applicable for practicable geometries. Because the derivation requires two spatial operations (the filter and the coordinate transformation), the curvilinear form cannot be acquired in a unique manner. By contrast, an order of operations does not arise when transforming a Reynolds-averaged Navier–Stokes (RANS) set of equations (or, for that matter, a direct numerical simulation system of equations) because only that single spatial operation in needed to arrive at the final generalized form. The question to be answered in the present derivation is whether one should filter the full-resolution equations before or after the coordinate transformation. This order especially effects implementation of the SGS model and even more importantly mixed modeling concepts where the Leonard term is evaluated explicitly.

Two procedures will be considered herein for obtaining a LES curvilinear coordinate form. Each approach will operate on the Navier–Stokes (NS) equation system of an incompressible flow. The first procedure filters the Cartesian coordinate system prior to its transformation. The order of operations respectively appears as

$$\text{NS (Cartesian)} \Rightarrow \textbf{Filter} \Rightarrow \text{LES (Cartesian)} \Rightarrow \textbf{Transform} \Rightarrow \text{LES (curvilinear)}.$$

This path is customarily taken when deriving a RANS type formulation but with the spatial filter operation replaced by Reynolds time-averaging. An alternative progression to this path involves reversing the order of operations. This second derivation proceeds as

$$\text{NS (Cartesian)} \Rightarrow \textbf{Transform} \Rightarrow \text{NS (curvilinear)} \Rightarrow \textbf{Filter} \Rightarrow \text{LES (curvilinear)}$$

such that the filter operation is now sensibly directed along the grid lines. To justify this latter choice, satisfaction of the commutative property is required between the filtering and the transformed form of the differentiation. Since the transformations occur before filtering, the accompanying metrics are depicted as filtered quantities. This viewpoint requires explanation and opposes the unfiltered representation of the first approach, where the order of operations is reversed. The following work will also show that the second choice greatly facilitates implementation of the final LES equations as well as explicit evaluation of the Leonard term.

Mathematically, the two paths just mentioned differ only by their formal appearance which is centered on the definition and evaluation of the transformation metrics. At the

outset, the resultant formulations reveal very little regarding their intrinsic separation of the large- and small-scale eddies. We must therefore understand the underlying mechanism of filtering along the curvilinear lines in either the physical domain or transformed space as well as interpret the physical significance of the transformation operation on the resolved and modeled fields. Thus, the primary objectives of this work include; formulating and interpreting a LES methodology suitable for incompressible flows in complex geometries (Section 2), designing a numerical filter kernel for explicit evaluation of the Leonard term (Section 3), and "a-priori" testing of the new LES formulation using a germane database (Section 4). Finally, a few important closing comments are presented regarding the turbulent eddy viscosity models commonly used for the SGS field (Section 5).

II. CURVILINEAR COORDINATE FORMULATION

To derive a generalized curvilinear coordinate formulation of LES equations for unsteady incompressible turbulent flows, we begin with the Cartesian system comprising the continuity and the Navier–Stokes equations. In nondimensional primitive variables, this system appears as

$$\text{Continuity} \quad \frac{\partial u_i}{\partial x_i} = 0 \tag{1}$$

$$\text{Momentum} \quad \frac{\partial u_i}{\partial t} + \frac{\partial u_j u_i}{\partial x_j} = -\frac{\partial p}{\partial x_j} + \frac{1}{\mathrm{Re}} \frac{\partial^2 u_i}{\partial x_j \partial x_j}, \tag{2}$$

where Re symbolizes the Reynolds number and u_i $(i = 1, 2, 3)$ and p represent the velocity and pressure quantities, respectively. Solving these equations necessitates resolution of all the spatial scales of the turbulent field which is classified as a direct numerical simulation (DNS). One can now choose to either filter this DNS system, followed by a transformation operation, or vice versa to acquire a LES formulation in generalized curvilinear coordinates. The resultant equations differ only by their mathematical depiction of the metric quantities. We will first examine the former choice which is hereinafter referred to as the "conventional approach."

A. *Conventional Approach*

Under the conventional approach one derives the basic governing equations of the flow in Cartesian coordinates first, then transforms them to a curvilinear coordinate framework (ξ^k). This order of operations produces LES equations of the form

$$\frac{\partial \sqrt{g}\xi_i^k \bar{u}_i}{\partial \xi^k} = 0 \tag{3}$$

$$\frac{\partial \sqrt{g}\bar{u}_i}{\partial t} + \frac{\partial \sqrt{g}\xi_{x_j}^k \bar{u}_j \bar{u}_i}{\partial \xi^k} = -\frac{\partial \sqrt{g}\xi_{x_i}^k \bar{p}}{\partial \xi^k} + \frac{\partial \sqrt{g}\xi_{x_i}^k \tau_{ij}}{\partial \xi^k} + \frac{1}{\mathrm{Re}} \frac{\partial}{\partial \xi^k}\left[\sqrt{g} g^{k\ell} \frac{\partial \bar{u}_i}{\partial \xi^\ell}\right]. \tag{4}$$

Each term in these equations is shown in its nondimensional strong conservation-law form [5]. The coefficients $\xi_{x_j}^k$ (as well as $g^{k\ell}$) and $\sqrt{g}$ denote the contravariant metrics and the

Jacobian of the transformation, respectively. Inasmuch as the filter operation is performed prior to any coordinate transformations, only the flow quantities are treated as filtered (designated by the overbar). Consequently, the types of filter functions are identical to those commonly found in the literature for Cartesian coordinate systems [6]. Moreover, special concern about satisfying the commutative property between the filtering and the differentiation is not necessary. The SGS stress tensor (τ_{ij}) is defined by $\tau_{ij} = \bar{u}_j\bar{u}_i - \overline{u_j u_i}$. Its contravariant density form (τ_i^k) appears as

$$\tau_i^k = \sqrt{g}\xi_j^k(\bar{u}_j\bar{u}_i - \overline{u_j u_i}) \tag{5}$$

which is directed along the curvilinear grid lines.

In the above transformed system, the varying filter width (Δ_f) is assumed to be equal to the local grid spacing (Δ_g). Thus, the resolved and filtered turbulent scales are identical. If $\Delta_f > \Delta_g$, filtering the convective term introduces additional terms representative of the intermediate turbulent physics lying between the respective filtered and resolved fields. The SGS stress τ_i^k is replaced by the tensor

$$T_i^k = L_i^k - Q_i^k, \tag{6a}$$

where

$$L_i^k = \sqrt{g}\xi_{x_j}^k(\tilde{u}_i\tilde{u}_j - \overline{\tilde{u}_i\tilde{u}_j}) \tag{6b}$$

$$Q_i^k = \sqrt{g}\xi_{x_j}^k(\overline{u_i'\tilde{u}_j} + \overline{\tilde{u}_i u_j'} + \overline{u_i' u_j'}). \tag{6c}$$

Again, both tensors L_i^k and Q_i^k are conservative transformations of their Cartesian counterparts. The instantaneous velocities are decomposed into their resolved ($\tilde{u}_i$) and modeled (u_i') elements with the overbar still denoting the filter operation. The Leonard term (L_i^k) is evaluated explicitly, whereas a model must be devised for the new SGS tensor (Q_i^k) which now consists of the cross ($\overline{u_i'\tilde{u}_j} + \overline{\tilde{u}_i u_j'}$) and Reynolds stress ($\overline{u_i' u_j'}$) tensors.

There are many difficulties, however, when numerically implementing the above LES system over boundary-fitted grids in complex geometries, including its assessment of the approximation effects in wave-number space. First, the Leonard term would be cumbersome to evaluate consistently along the curvilinear lines because the filter operation is formally instituted in the Cartesian coordinate system. The filter kernel itself is improperly defined with its width especially onerous to determine locally. Moreover, the spectral physics of the Leonard term would be difficult to isolate from the neighboring attenuation of the convective term caused by its finite difference approximation.

Second, the absense of the overbar for each metric coefficient implies that they are evaluated exactly thereby vary monotonically. Although their analytical determination is certainly possible for strongly controlled grids, the order of the leading term in the truncation error of both the first- and second-order derivatives is actually reduced when compared to that obtained through their difference approximation. This convincing argument was presented in-depth by Thompson *et al.* [7] by simply examining the metric coefficient of the transformed first-order derivative. They showed that the leading term

of the respective truncation error reduces one order if the metric coefficient is evaluated analytically.

Third, although one can argue that certain monotonic functions can be useful for minimizing the truncation error, enforcing these distributions either locally or globally can be difficult and nearly impossible under an adaptive gridding computation. Vinokur [8] concluded that simple analytic evaluations of the metrics and Jacobian can improve the solution accuracy only for isolated cases, but that numerical treatment is generally preferred for most complex geometric applications.

To this end, the conventional approach can only be viewed as a useful LES methodology for complex domains if one ignores these salient drawbacks associated with its implementation. Specifically, the filter operation is ill-defined which further complicates spectral analysis of the results as well the numerical approximations. Furthermore, a comparatively lower-order truncation error arises because the final formulation implies that the metric coefficients are evaluated analytically rather than numerically.

B. *Alternate Approach*

An alternate sequence to the above involves reversing the order of operations which gives the LES equations

$$\frac{\partial \overline{\sqrt{g}\xi_i^k u_i}}{\partial \xi^k} = 0 \tag{7}$$

$$\frac{\partial \overline{\sqrt{g}u_i}}{\partial t} + \frac{\partial \overline{\sqrt{g}\xi_{x_j}^k u_j}\,\overline{u}_i}{\partial \xi^k} = \frac{\partial \overline{\sqrt{g}\xi_{x_i}^k p}}{\partial \xi^k} + \frac{\partial \tau_i^k}{\partial \xi^k} + \frac{1}{\mathrm{Re}}\frac{\partial}{\partial \xi^k}\left[\overline{\sqrt{g}g^{k\ell}\frac{\partial u_i}{\partial \xi^\ell}}\right]. \tag{8}$$

This second approach transforms the basic NS equations prior to their filtering. Consequently, the filter operation is now formally administered along the grid lines, where the independent spatial variables are the curvilinear coordinates. The filter operates on both the flow quantity and the metric coefficient. It is important to note that the finite-difference expressions used for approximating each metric coefficient are separate mechanisms of spatial filtering which justify representing them as filtered quantities in the basic formulation. For the moment, further discussion on this particular topic will be deferred until in the next section.

The filter operation along the curvilinear grid lines can be expressed as

$$\overline{g(\xi^k)\phi(\xi^k)} = \int H(\xi^k - \xi'^k) g(\xi'^k)\phi(\xi'^k)\, d\xi'^k, \tag{9}$$

where $H(\xi^k - \xi'^k)$ is the homogeneous filtering kernel, $g(\xi'^k)$ is the metric coefficient, and $\phi(\xi'^k)$ is an arbitrary turbulent quantity. The coefficient $g(\xi'^k)$ transforms $\phi(\xi'^k)$ to the curvilinear coordinate system such that their product becomes the contravariant counterpart of the quantity. Filtering can occur in either the physical domain or the computational space with both applications having characteristic filter widths defined by the local metric coefficient (see Fig. 1). For instance, the grid-filter width along the η lines (η is constant) in the physical domain is the local metric coefficient $\sqrt{g_{11}}$. Commutation between filtering and the finite difference approximations along nonuniform grid spacing was argued by Moin and Kim [9]. They satisfied this property by treating their second-order central scheme as

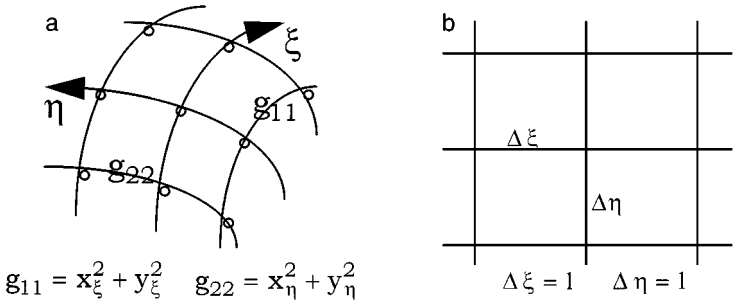

FIG. 1. Filtering along the curvilinear lines: (a) physical domain; (b) computational space.

a sectional box filter kernel applied locally at each computational point. However, Ghosal and Moin [10] later noted that filtering an arbitrary quantity in the physical domain under nonuniform spacing theoretically violates the commutative property between the filter operation and the differentiation. In their analysis, the filter kernel was considered transformed rather than the flow variable. They concluded that the associated error will not contaminate the methodology, however, if the numerical approximations are no higher than second order.

With the filter kernel herein defined in curvilinear coordinates, one can easily show that the differentiation and the filtering commute for each transformed term in the computational space. Consider, for example, the one-dimensional differentiation of (9) as

$$\frac{d\overline{[g(\xi)\phi(\xi)]}}{d\xi} = \int \frac{d[H(\xi-\xi')]}{d\xi} g(\xi')\phi(\xi')\,d\xi', \tag{10}$$

where the filter width $\Delta = \delta\xi = 1$. Integration by parts will prove that

$$\frac{d\overline{[g(\xi)\phi(\xi)]}}{d\xi} = \overline{\frac{d[g(\xi)\phi(\xi)]}{d\xi}} + H(\xi-\alpha)g(\alpha)\phi(\alpha) - H(\xi-\beta)g(\beta)\phi(\beta), \tag{11}$$

where α and β define the geometric limits of the space. Thus, filtering and the differentiation commute in the computational space with the stipulation that the terms $g(\alpha)\phi(\alpha)$ and $g(\beta)\phi(\beta)$ (or their difference) vanish at the boundaries.

The SGS stress field shown in Eq. (8) assumes that the filter operates implicitly through the spatial resolution of the implemented grid ($\Delta_f = \Delta_g$). As noted earlier, those scales captured by the grid spacing hold all the resolved portion of the turbulence. This viewpoint can be theoretically interpreted as applying a sharp cutoff filter along the curvilinear lines in wave-number space such that the separation of the resolved and modeled fields becomes distinct. The Leonard term is eliminated ($\tilde{u}_i = \bar{u}_i$) and the SGS field is defined as

$$\tau_i^k = \overline{\sqrt{g}\xi_j^k u_j}\bar{u}_i - \overline{\sqrt{g}\xi_j^k u_j u_i}. \tag{12}$$

This field represents the fine-scale turbulent eddies along the curvilinear grid lines which requires derivation of a physics-based model.

Before proceeding further, the contravariant velocity components can be introduced to simplify the LES equations. Moreover, each metric coefficient can be declared filtered and independent from its respective resolved turbulent quantity because the metrics should

be conceived as smooth functions which are evaluated numerically and devoid of any fluctuations. The resolved contravariant velocity components ($\overline{U^k}$) are defined as

$$\bar{U}^k = \overline{\sqrt{g}\,\xi^k_{x_j}}\,\overline{u_j} \tag{13}$$

because $(\sqrt{g})' = (\xi^k_{x_i})' = 0$. Substituting this expression into Eqs. (7) and (8) gives

$$\frac{\partial \overline{U^k}}{\partial \xi^k} = 0 \tag{14}$$

$$\frac{\partial \overline{\sqrt{g}}\,\overline{u_i}}{\partial t} + \frac{\partial \overline{U^k}\bar{u}_i}{\partial \xi^k} = \frac{\partial \overline{\sqrt{g}}\,\overline{\xi^k_{x_i}}\,\bar{p}}{\partial \xi^k} + \frac{\partial \sigma^k_i}{\partial \xi^k} + \frac{1}{\mathrm{Re}}\frac{\partial}{\partial \xi^k}\left[\overline{\sqrt{g}}\,\overline{g^{k\ell}}\frac{\partial \bar{u}_i}{\partial \xi^\ell}\right], \tag{15}$$

where σ^k_i is expressed as

$$\sigma^k_i = \overline{U^k}\overline{u_i} - \overline{U^k u_i}. \tag{16}$$

This tensor has an identical form to its Cartesian analogue, but it requires an exchange of variables to introduce the contravariant velocity components in the definition. Finally, introduction of the contravariant velocity into the Leonard term yields

$$L^k_i = \overline{\tilde{U}^k \tilde{u}_i} - \tilde{U}^k \tilde{u}_i \tag{17}$$

which can be easily evaluated explicitly along the curvilinear lines in either the physical domain or contravariant space using an appropriately designed filter.

III. CURVILINEAR LINE FILTERING

Although the filter operation is directed along the curvilinear grid lines, we can still argue for the same kernel functions that are used with Cartesian coordinate systems, except now the independent variables are the curvilinear coordinates. The most common functions are those of the sharp cutoff, Gaussian, and box filters. We will first direct our attention to the implicit filtering along the curvilinear lines that is associated with numerical evaluation of the coefficient metrics, followed by application of a box or Gaussian filter for explicit evaluations of the Leonard term.

A. *Implicit Filtering of the Metric Coefficients*

As noted earlier, if the transformation operation is performed prior to filtering, then each metric coefficient should be considered as a filtered quantity. This representation is justified herein due to the implicit filtering inherent in evaluating each coefficient by finite difference schemes. For example, numerical approximation of the metric coefficient x_ξ by second-order central differences carries a builtin box-type filter of unit width $\delta\xi$. The exact relation between this differencing scheme and the box filter is

$$x_\xi \approx \frac{x(\xi+1) - x(\xi-1)}{2} = \frac{\delta}{\delta\xi}\left\{\frac{1}{2}\int_{\xi-1}^{\xi+1} x(\xi)\,\delta\xi\right\} = \frac{\delta \bar{x}}{\delta\xi}, \tag{18}$$

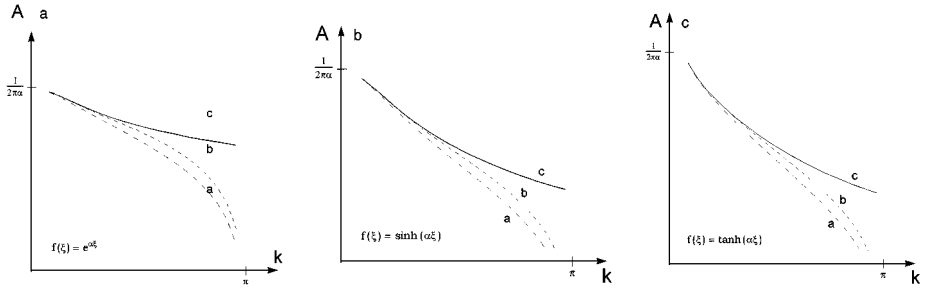

FIG. 2. Attenuation of the Fourier amplitudes of three stretching functions caused by finite difference approximations of the respective metric coefficients: (a) exponential; (b) hyperbolic sine; (c) hyperbolic tangent.

where the integral form of the box filter is shown in the parentheses. This filter will dampen the spectral components of the dependent Cartesian coordinate (x) in wave-number space (k), according to the response function $R(k) = \sin(k)/k$.

To illustrate the attenuation effect of the difference approximation in (18) on the metric coefficients, we will examine three monotonic expressions which are most commonly used to stretch the grid: the exponential, hyperbolic sine, and hyperbolic tangent functions [7] (i.e., $x(\xi) = e^{\alpha\xi}$). Attenuation of the respective Fourier amplitudes of the physical coordinate due to a two-point approximation of its derivative x_ξ is shown in Fig. 2 as curve (a); the maximum scaled wave-number ($k = 2\pi n/N$) of each function is π, $N+1$ is the number of grid points, and $1 \le n \le N/2$. In this figure, the exact Fourier amplitudes (no filtering) of each distribution are designated by curve (c). One can see that significant attenuation of the spectral components begins at very low wave-numbers independent of the grid point distribution. At $k = \pi/2$, for example, each Fourier amplitude is damped by about 34%. Curve (b) illustrates the damping effect caused by a fourth-order-accurate central scheme. At a minor cost of additional CPU time, one can delay significant damping of the Fourier amplitudes of the Cartesian coordinate until higher wave-numbers.

Higher order difference approximations and compact schemes will still further relax realizable attenuation of the spectral amplitudes of the physical coordinate, but complete elimination is not achievable. Thus, considering each metric coefficient as a filtered variable in the alternate approach is justified, due to the implicit spatial filtering that occurs through its numerical evaluation.

B. *Explicit Filtering*

When $\Delta_f > \Delta_g$, the Leonard term of (17) arises in the alternate LES formulation that must be evaluated explicitly in the computation. A filter can be designed for this purpose that is executed in either the physical domain or the computational space. As previously noted, filtering in the physical domain must be in accordance with a second-order discretization of the governing terms to minimize the commutation error. Although the filter in the physical domain is slightly more costly to apply (due to the nonuniformity of grid spacing), both filter kernels have similar forms. The primary difference between the two filter operations lies not in the filter definition itself but in the variable being filtered. In the computational space, pre and posttransformations are required so that concerns arise about its relative CPU cost and energy conservation properties. Furthermore, one should exert caution for highly stretched grids because the filtered metric coefficient drastically dampens the contravariant

form of the filtered flow variable. In this section, two kernels are examined of the box filter (one for each domain) that essentially implements volume-averaging [11]. These kernels will then be tested in the following section to study their relative damping effects on the turbulent spectral energy.

The basic kernel of the box filter has the conservative functional form

$$H(\xi^k, \xi'^k) = \begin{cases} 2/(\Delta_i^+ + \Delta_i^-), & \text{if } \Delta_i^-/2 < |\xi^i - \xi'^k| < \Delta_i^+/2 \\ 0, & \text{otherwise} \end{cases}, \tag{19}$$

where Δ_i is the local filter width in the curvilinear direction ξ^k. Direct application of this filter to an orthogonal boundary-fitted grid in the physical domain gives $\Delta^2 = g_{11}$ and $\Delta^2 = g_{22}$ in the ξ and η directions, respectively (see Fig. 1). In the computational space, $\Delta = 1$ everywhere because the associated grid is completely uniform.

The analog of discrete volume averaging along a curvilinear line in the computational space has the form

$$\bar{\phi}_i = \phi_i + S/2[\phi_{i+1} + \phi_{i-1} - 2\phi_i], \tag{20}$$

where S is the filter coefficient. To ensure that this operation attenuates the Fourier elements without a phase change, the filter coefficient is simply set to $1/2$ [12]. Damping the high wave-number spectral amplitudes of the metric coefficients using this operation depends strongly on the local degree of stretching. To illustrate this point, consider the filter operation rewritten as

$$\bar{\phi}_i = \phi_i + \frac{S}{2}\frac{d^2\phi}{d\xi^2}, \tag{21}$$

where the second-order term is consistent with second-order discretization. Using the previous three monotonic functions, the filtered metric coefficient $\bar{x}_\xi$ relative to its unfiltered component becomes

$$\bar{x}_\xi = x_\xi(1 + \beta), \tag{22}$$

where the smoothing parameter β is defined as

$$\beta = Sq'''/2q' \tag{23}$$

and the variable q denotes the distribution function (i.e., $q' = x_\xi = \alpha e^{\alpha\xi}$). The relative degree smoothing of the metric coefficients using these functions is listed in Table I for two extreme cases of grid stretching. The first case restricts the grid stretching to minimize the truncation error of standard second-order central differences applied to the metric coefficients. The respective smoothing is minimal for all three distributions, suggesting that the resultant damping of the spectral amplitudes of the metric coefficients by the operation in (20) is negligible. But this stretching restriction is unrealistic, and it is rarely encountered throughout most boundary-fitted grids. The other case illustrates strong damping when the subsequent grid point spacing is doubled. Although this stretching exceeds that allowable by the truncation error of most finite difference schemes, the hyperbolic functions appear least affected by filtering. These particular monotonic distributions have been identified as the best overall choices for resolving bounded shear layers [8].

TABLE I
Smoothing Effects of Box Filtering

Function $q(\xi/N)$	Degree of grid stretching			
	$(x_\xi)_2/(x_\xi)_1 = 1 + (x_\xi)_1$		$(x_\xi)_2/(x_\xi)_1 = 2$	
	α	β	α	β
$\frac{\exp(\alpha\xi/N)-1}{\exp\alpha - 1}$	0.42	$O(10^{-2})$	1.39	$O(1)$
$\frac{\sinh(\alpha\xi/N)}{\sinh\alpha}$	1.24	$O(10^{-1})$	1.92	$O(10^{-1})$
$1 - \frac{\tanh[\alpha(1-\xi/N)]}{\tanh\alpha}$	0.92	$O(10^{-1})$	1.26	$O(10^{-1})$

Note. $(x_\xi)_1$ signifies local grid spacing at the first point, q is the distribution function, and N is the total number of points ($N = 2$).

Most importantly, with strict control over excessive grid stretching the implications of smoothing the metric coefficients (through explicit filtering) does not alter the basic physical processes intrinsic in the LES computations. For instance, the Leonard term provides substantial assistance towards the forward scatter of energy from the finest resolved scales to the coarsest subgrid eddies. For uniform grid spacing, spectral analyses of the energy cascade process to quantify the Leonard term contributions is simply illustrated at the discrete wave-numbers. This same process occurs along the curvilinear lines at modified wave-numbers because the respective wave-lengths have been smoothed. Although we expect the differences to be minor, the extent depends largely on the degree of relative stretching. In view of the turbulent energy, the spectral amplitudes are damped further by a factor proportional to β.

In the physical domain, we can locally account for the nonuniform grid spacing by introducing a weighting function (a),

$$\bar{\phi_i} = \phi_i + S/(1+a)[\phi_{i+1} + a\phi_{i-1} - (1+a)\phi_i]. \tag{24}$$

The magnitude of the corresponding response function $|R(k)|$ is

$$|R(k)| = 1/2(1+a)\left\{[(1+a)(1+\cos k)]^2 + [(1-a)\sin k]^2\right\}^{1/2} \tag{25}$$

which dampens all Fourier components except at wave-number $k = 0$. As illustrated in Fig. 3, the effect of the weighting function is additional damping of the high wave-number spectral components. Expanding this filter to three dimensions (3D) produces a 27-point operator of the form

$$\begin{aligned}\bar{\Phi}_{i,j,k} = {} & \Phi_{i,j,k} + D_1[(1+a)(\Phi_{i,j+1,k} + b\Phi_{i,j-1,k}) + (1+b)(\Phi_{i+1,j,k} + a\Phi_{i,j-1,k})] \\ & + D_2[(1+a)(\Phi_{i,j+1,k\pm1} + b\Phi_{i,j-1,k\pm1}) + (1+b)(\Phi_{i+1,j,k\pm1} + a\Phi_{i-1,j,k\pm1})] \\ & + D_2[\Phi_{i+1,j+1,k} + a\Phi_{i-1,j+1,k} + b\Phi_{i+1,j-1,k} + ab\Phi_{i-1,j-1,k})] \\ & + D_3[\Phi_{i+1,j+1,k\pm1} + a\Phi_{i-1,j+1,k\pm1} + b\Phi_{i+1,j-1,k\pm1} + ab\Phi_{i-1,j-1,k\pm1})],\end{aligned} \tag{26}$$

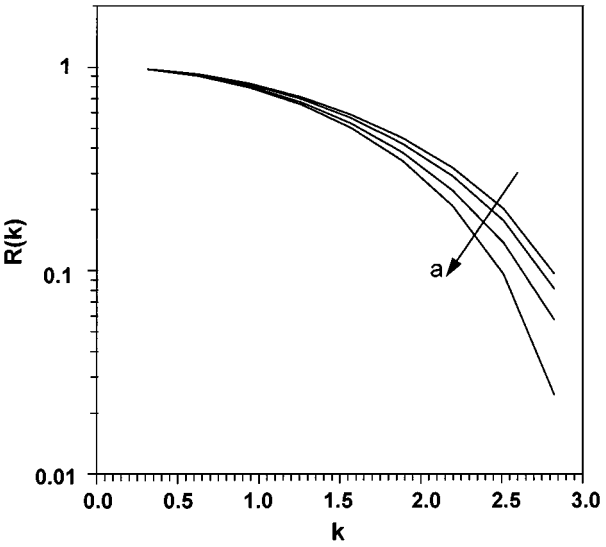

FIG. 3. Additional damping of a filtered quantity caused by local weighting.

where

$$D_1 = S(1-S)^2/2(1+a)(1+b)$$
$$D_2 = S^2(1-S)/2(1+a)(1+b)$$
$$D_3 = S^3/2(1+a)(1+b).$$

In the physical domain, the grid's nonuniformity is embedded in the neighboring parameters $a = \sqrt{g_{11}^+/g_{11}^-}$ and $b = \sqrt{g_{22}^+/g_{22}^-}$ in the ξ and η directions, respectively. In the computational space, these parameters are unit-valued. No weighting parameter reflects differences in the spanwise spacing (z, ζ coordinates) because it is assumed to be uniform for the present application.

Finally, one could easily select a Gaussian functional instead of the box kernel to explicitly filter the contravariant components. When administered in the computational space, this filter would have the same basic form as the one used by Leonard [6], but with unit filter width. The Gaussian filter (G^k) in this application appears as

$$G^k = \left(\frac{6\alpha^2}{\pi}\right)^{3/2} e^{-6[\alpha(\xi^k - \xi^{k'})]^2}. \tag{27}$$

with $\alpha = 1/2$. Like the box filter, attenuation of all the spectral elements of the transformed variable will occur except at the corresponding zeroth wave-number. However, the energy loss is generally less severe when compared directly to that resulting from the box filter.

IV. *A PRIORI* TESTING AND DISCUSSION

In this section, *a priori* tests are performed on a turbulent flow for the purpose of investigating the relative damping of the spectral components in the proposed formulation and to further decide which grid-filter is best suited for computing the Leonard term. These tests

reflect DNS results collected of a circular cylinder wake at a subcritical Reynolds number of 3400, based on the cylinder diameter (D). This particular Re was chosen because the experimental flow visualization results of Wei and Smith [13] showed little development of the fine-scale spanwise cellular deformation of the shed Strouhal vortices. This observation selectively eased the spanwise resolution requirement of the structured grid. Statistically, the Strouhal number (S_t) of this flow is close to 0.2 [14]; $S_t = fU/D$, where U is the freestream velocity and f is the shedding frequency of the primary vortices.

To acquire the DNS results of the cylinder wake, the fractional-step formulation of Jordan and Ragab [15] was recast into generalized curvilinear coordinates. Their technique is an extension of the DNS finite-difference scheme of Rai and Moin [16] to a semi-staggered discretization molecule. Third-order upwind-biased differences approximate the convective derivatives in the wake streamwise and transverse directions (ξ, η lines) to inhibit aliasing and stabilize the computations in the downstream coarse grid regions near exit. The periodic spanwise components are approximated by a fourth-order accurate compact scheme [17]. A Runge–Kutta procedure is used to time-advance the flow because of its strong numerical stability even under inviscid conditions. The viscous terms are time-split by the Crank–Nicolson scheme and spatially approximated by conservative finite-volume differences. The overall accuracy of the solutions are second order in both space and time.

A. *Grid Resolution and Boundary Conditions*

For the turbulent cylinder wake, the finest dissipation scales occur within the vortex formation region. To ensure sound resolution of this region, various curvilinear grids were tested for increased refinement until the relative prediction of Kolmogorov's microscale fell below 2%. The final grid, along with the external boundary conditions, are given in Fig. 4. An exponential interpolation function was used to uniformly cluster the η lines toward the cylinder surface. The radial ξ lines emanated normally from the cylinder periphery (s) and were uniformly distributed circumferentially around the cylinder ($\Delta s \approx 0.008\pi$). This control produced a single-valued covariant metric coefficient along these concentric lines which further facilitated spectral analyses of the box and Gaussian filters. The spanwise resolution

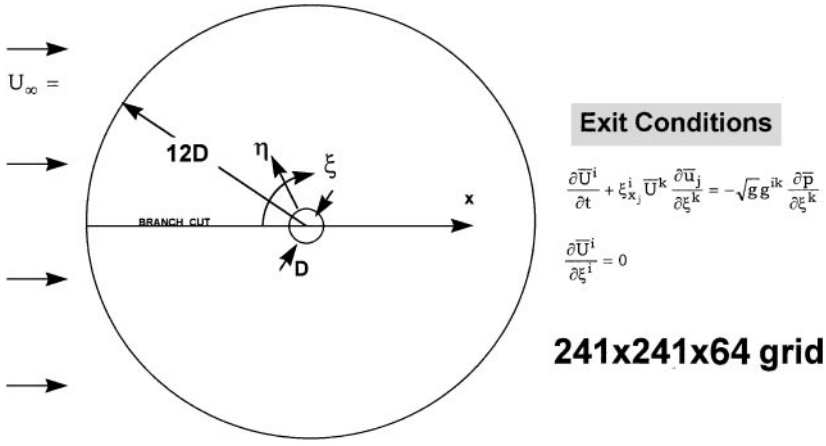

FIG. 4. Grid line distribution, external boundaries, and flow conditions used for direct numerical simulation of cylinder flow at Re = 3400.

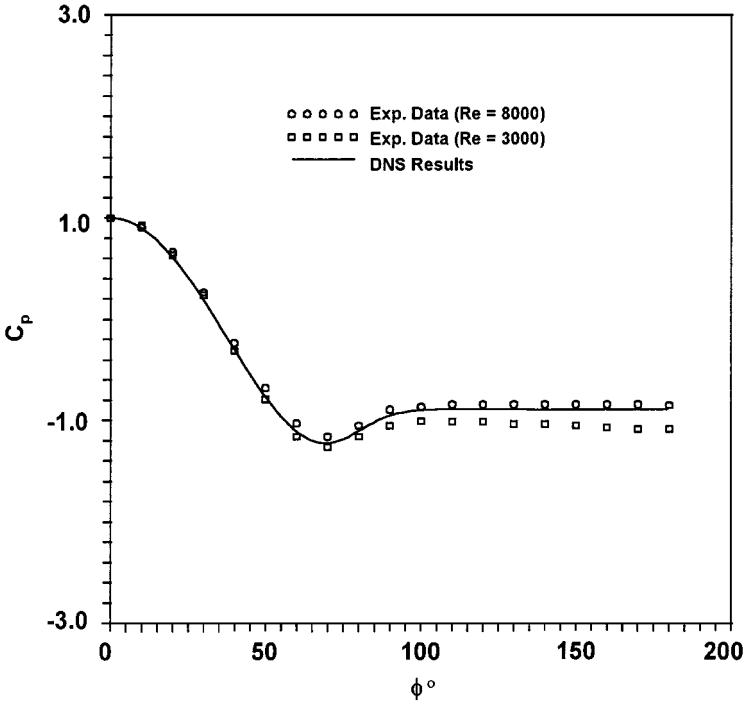

FIG. 5. Comparison of the mean pressure coefficient from the DNS results to the experimental data reported by Norberg [20].

was based on the empirical relationship of Mansey *et al.* [18] for the wavelength (λ_z) of the three-dimensional disturbances; $\lambda_z/D \sim 20\mathrm{Re}^{-1/2}$. Using 64 points over π length, the DNS computation gave approximately seven points for resolving each disturbance. Moreover, this spanwise resolution produced an accurate prediction of the base pressure coefficient immediately downstream of the cylinder (see Fig. 5). Finally, the combined transformed forms of the continuity and Euler equations were found satisfactory for applying a velocity condition to exit the shed vortices with minimum distortion [19].

To illustrate the resolution capacity of the grid, phase-averaged results (at the shedding frequency) of Kolmogorov's microscale (η_d) are shown in Fig. 6. Homogeneous conditions

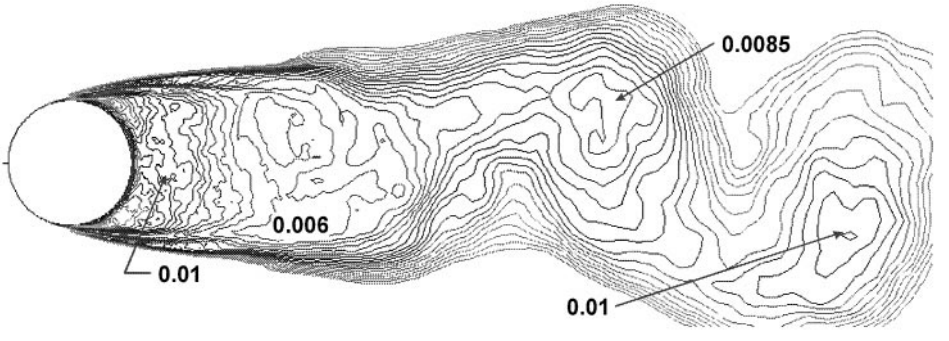

FIG. 6. Phase-averaged DNS results of Kolmogorov's microscale in cylinder wake at Re = 3400; contours increment by 0.0005.

TABLE II
Kolmogorov Microscale and Grid Density in Kolmogorov Units at $x/D = 5$

$\eta_d^e/D \times 10^3$	$\eta_d^n/D \times 10^3$	$\sqrt{g_{11}}/\eta_d^e$	$\sqrt{g_{22}}/\eta_d^e$	$\Delta z/\eta_d^e$
9.84	14.53	13.74	7.38	4.99

Note. η_d^e/D is the experimental measurement at $\mathrm{Re} = 3900$ [21] scaled to $\mathrm{Re} = 3400$ and η_d^n/D is the DNS computation at $\mathrm{Re} = 3400$.

were assumed in the spanwise direction. In the figure, η_d is scaled by the cylinder diameter leading to the definition

$$\eta_d/D = (1/\mathrm{Re}|S|)^{1/2}, \tag{28}$$

where $|S|$ denotes the magnitude of the transformed resolvable strain-rate tensor. As expected, the finest turbulent scales were computed within the vortex formation region; $0.004 < \eta_d/D < 0.01$. Conversely, negligible turbulent levels are indicated outside the near wake and in the upstream flow. The phase-averaged results clearly show an increase in η_d/D toward the primary vortex cores. This result agrees qualitatively with our understanding that the shed vortices, which are turbulent, have viscous cores which tend towards relaminarization.

Within the vortex street, specific evidence to demonstrate the grid's ability to adequately resolve the dissipation scales is shown in Table II. At 5 diameters downstream, the table lists the mean experimental measurement $\eta_\mathrm{d}^\mathrm{e}/\mathrm{D}$ [21] and the present DNS result η_d^n/D, along with the local grid densities in experimental Kolmogorov units. Note that the experimental measurements were taken at $\mathrm{Re} = 3900$, but scaled to the DNS computation assuming the wake turbulence is homogeneous and isotropic ($\propto \mathrm{Re}^{3/4}$). In view of the resolution requirements discussed by Reynolds [22], the grid densities at $x/D = 5$ were sufficient for the DNS computation.

The near wake turbulent spectral energy versus streamwise wave-number (both in Kolmogorov units) is shown in Fig. 7. Ong and Wallace [21] converted their experimental frequency spectrum to the one-dimensional wave-number spectrum shown in the figure using Taylor's hypothesis. Although their profile is specifically taken from the LDV data at $x/D = 3.0$ and $y/D = 0.56$, the curve is representative of the entire near-wake regime. Superimposed on the profile are the present DNS results (corrected for the Re difference) at $r/D = 1.54$ (formation region) and $r/D = 5.0$ (vortex street), as well as the LES results of Beaudan and Moin [4] at $x/D = 5.0$. Unlike the LES results, neither DNS curve suggests a dampening or dumping of turbulent energy at the higher resolved wavenumbers. This result is probably attributed to the DNS grid supplying 61 and 36% finer spatial resolutions than the LES grid at the downstream locations of $x/D = 1.54$ and $x/D = 5.0$, respectively.

Finally, comparisons of the DNS turbulent statistics within the formation region ($x/D = 1.54$) and the vortex street ($x/D = 4.0$) to the PIV data of Lourenco and Shih [4] and the LES results of Beaudan and Moin [4] are illustrated in Fig. 8. To account for the difference in Reynolds numbers, both the turbulent means and intensities are scaled by the local streamwise defect velocity (u_d). In view of the measurement uncertainty [4], the present DNS computations agree favorably with the observations. The transverse turbulent intensities show closer agreement to the experimental evidence than the results of Beaudan

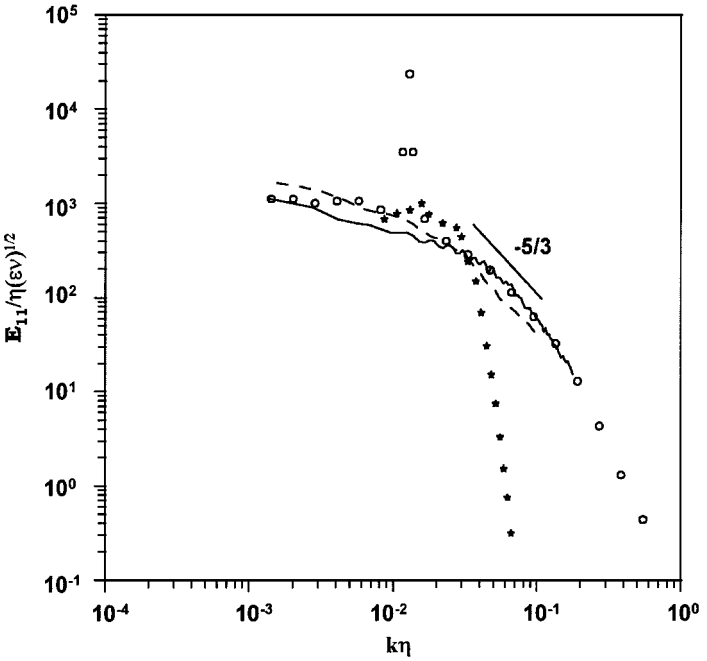

FIG. 7. A comparison of turbulent energy spectrum versus wavenumber (both scaled in Kolmogorov units); ——— and - - - -, present DNS at $r/D = 1.54$ and $r/D = 5.00$, respectively; ○○○○, experimental data [21]; ★★★★★, LES results [4].

and Moin, who used fifth-order upwind-biasing for the convective derivatives coupled with a dynamic SGS model. As previously noted, the present DNS results reflect computations performed over a much finer grid. Given this agreement with the experimental evidence, the present DNS results within the formation region were consider satisfactory for subsequent analysis of the box filters and Leonard term of the alternate LES formulation.

B. *Explicit Filtering Along the Curvilinear Lines*

The higher CPU efficiency and energy-conservation of box filtering in the transformed space, compared to the results from the physical domain filter (Eq. (26)), is illustrated in Figs. 9a and 9b. Both profiles represent four phase-averaged datasets saved at the shedding frequency, as well as spatial averages in the spanwise direction. The box filters were applied along the η line corresponding to the radius $r/D \cong 0.69$ with filter widths set at twice the local grid spacing. This particular concentric line lies within the well-resolved vortex formation region shown earlier. Its end conditions are periodic due to the branch-cut implemented upstream. Both filters show substantial damping of the spectral energy (E_{22}) within the inertial subrange. Notice that no differences in the damped levels are observable between each filtering scheme. The expanded profiles (Fig. 9b), that focus on the dissipation range, further emphasize this point. Conversely, the computational cost of the physical domain application is nearly twice that of the computational space, even including the added expense associated with the transformation operation. This comparatively lower efficiency of the physical domain filter is attributed to its direct dependence on the local weighting functions.

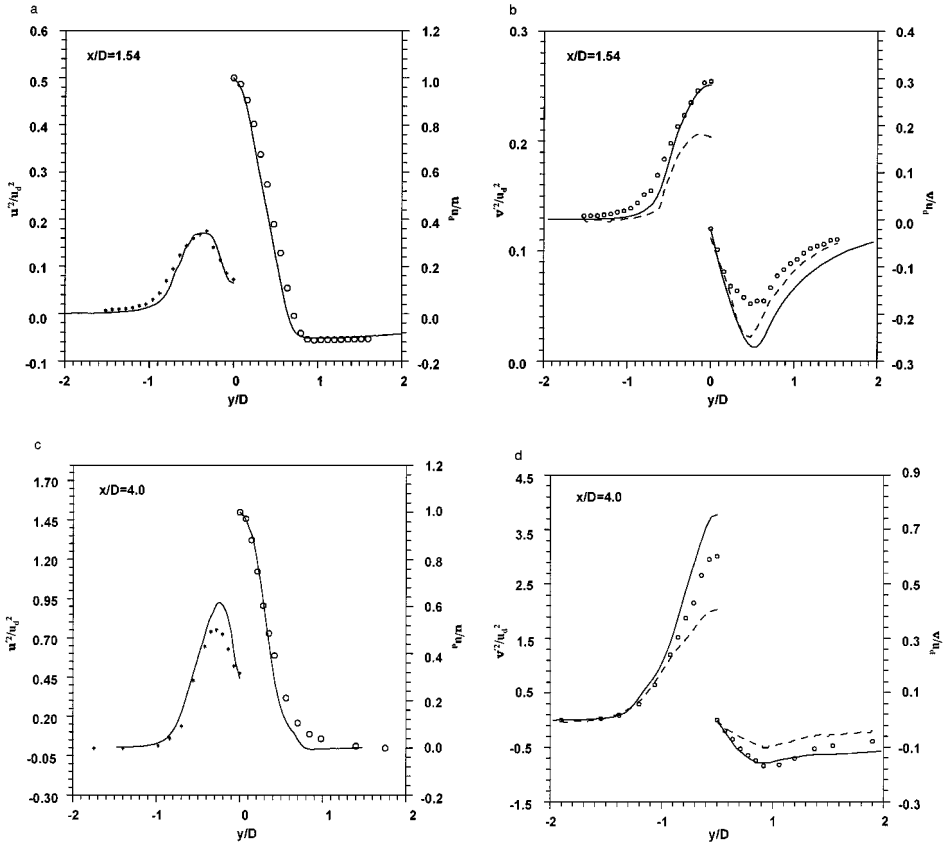

FIG. 8. Comparisons of the streamwise and transverse mean velocity (u, v) and total Reynolds stresses ($\mathbf{u}'^2\mathbf{v}'^2$) given by the present DNS results (solid lines) to experimental (circles and asterisks) and LES data (dashed lines) reported in [21] and [4], respectively.

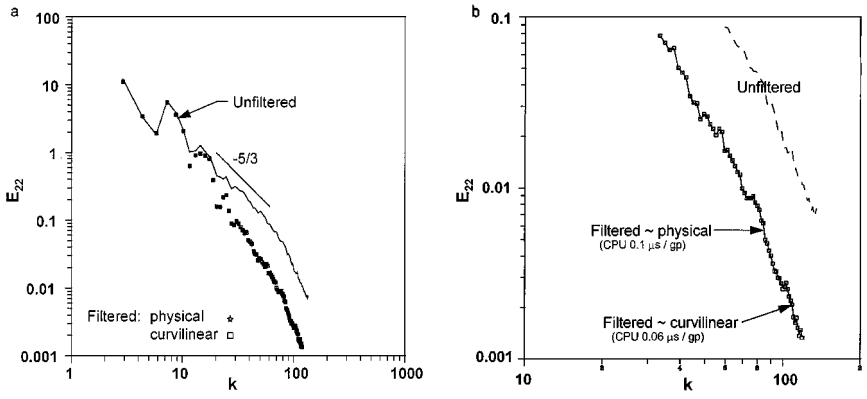

FIG. 9. Comparisons of the damping effects on the spectral energy caused by the explicit box filters designed for application in the physical domain and computational space (Re = 3400).

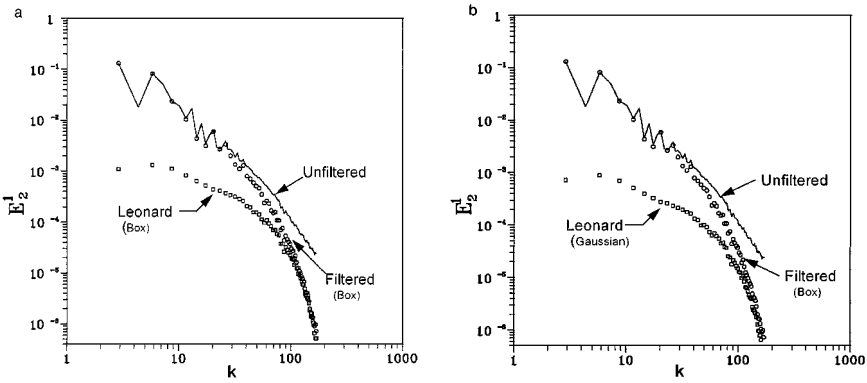

FIG. 10. Comparisons of the Fourier components of the filtered transformed Leonard stress L_2^1 to the spectral energy of the box filtered component $\bar{U}\bar{v}$; $L_1^2 = \overline{U\bar{v}} - \bar{U}\bar{v}$: (a) box filtered L_2^1, $r/D = 0.69$; (b) Gaussian filtered L_2^1, $r/D = 0.69$.

C. *Leonard Term*

When $\Delta_f > \Delta_g$, one must ensure that the Leonard term is not masked by a low-order approximation of the flux derivatives. In particular, if the convective flux is approximated using three points, then the respective truncation error will be on the same order as the Leonard term. Inasmuch as the recommended governing LES equations are placed in conservative form, explicit evaluation of the Leonard stress actually includes approximating and filtering the metric coefficients. The correct procedure requires transforming each component to the computational space prior to their filtering. The contributions of the Leonard term relative to the convective flux depend on the smoothing and order-of-accuracy of the respective metric coefficients.

In terms of an energy loss, box filtering the contravariant DNS components is equivalent to a finite-volume second-order approximation of the transformed flux derivatives in the LES computation with $\Delta_f = \Delta_{\text{LES}} = 2\Delta_{\text{DNS}}$. This analogy is strictly numerical, however, because the resolved field will dynamically adjust itself to the SGS model over time. With this understanding, we can still allow a careful look at the relative importance of Leonard term. The procedure is similar to the *a priori* tests conducted by Liu *et al.* [23] and others [24, 25] using a top-hat filter. For instance, Figs. 10a and 10b show the spectral components of the Leonard term L_2^1 using either a box or Gaussian filter relative to the resolved component $\tilde{U}\tilde{v}$; $L_2^1 = \overline{\tilde{U}\tilde{v}} - \tilde{U}\tilde{v}$ along concentric line $r/D = 0.69$. The associated metric coefficients of the contravariant velocity components were approximated to the second-order. Both figures clearly show that a low-order scheme will prohibit any contributions from the Leonard stress near the higher wave-number part of the spectrum. The choice of the filter kernel does not seem to matter nor does the local grid spacing. Also, an improved fourth-order approximation of the metric coefficients leads essentially to the same conclusion. These results suggest that high-order finite difference schemes must be used for approximating the convective derivatives in the alternate LES formulation to indulge participation of the Leonard stress near the higher range of resolved wave-numbers.

V. FINAL REMARKS

Difficult geometries are commonplace among most practical applications. Consequently, to compute the respective turbulent physics one must utilize a generalized curvilinear

coordinate system to steer the flow solutions in conformance with the wall boundaries. Unlike the solution philosophies of a direct numerical simulation (DNS) or a Reynolds-averaged Navier–Stokes (RANS), the large-eddy simulation (LES) methodology centers on the fact that two spatial operations are formally necessary to arrive at a generalized formulation. Besides the coordinate transformations, one must spatially filter the mathematical system as well. The recommended order-of-operations is to transform the full-resolution equation system first, then filter the result. This sequence logically conforms the filter operation to the curvilinear field lines, but requires representing the coefficient metrics as filtered quantities. That demand is met implicitly through their numerical approximation. Numerical treatment of the metric coefficients is actually preferred over an analytical evaluation to minimize the associated truncation error.

Ghosal [26] recommends a grid-filter width larger than the local grid spacing to maintain dominance of the SGS model over the dispersive truncation error of an upwind-biased scheme for the convective derivatives. This advice demands development of a useful filter for explicit evaluation of the Leonard term. Because the grid spacing is nonuniform in the physical domain, explicit spatial filtering will cost more, relative to simple geometries, especially when evaluating the SGS field. Herein, grid-filtering in the computational space proved to be comparatively cheaper than in the physical domain with no discernible differences in the respective damped spectral energies.

For simple geometries, it is well known that the truncation error of a low-order approximation of the convective derivatives will overwhelm the Leonard term. Using a DNS database of the near wake of a circular cylinder, this presumption was verified in the computational space as well. Meaningful contributions from the Leonard stress in transformed coordinates are important only when the neighboring derivatives are approximated by high-order-accurate schemes. This fact also includes high-order treatment of the metric coefficients.

Finally, validating a curvilinear coordinate formulation for the SGS model is an issue for future work. Currently, Smagorinsky's dynamic form is the most popular for general applications involving complex turbulent flows. Its implementation requires test-filtering the resolved field which permits energy backscatter physics from the modeled scales to the finest resolved scales. However, previous studies conclude that Smagorinsky's model correlates poorly with the exact stress [23]. A family of alternatives have been proposed, but the related mixed model (similarity plus Smagorinsky relationships) probably shows the most promise. For practical geometries, this model appears to be CPU-intensive, due to its mathematical complexities.

ACKNOWLEDGMENTS

The author gratefully acknowledges the support of the Office of Naval Research (Contract No. N0001497-WX20346; Dr. L. P. Purtell, Program Officer) and the In-house Laboratory Independent Research Program (Dr. S. Dickinson, Coordinator) at the Naval Undersea Warfare Center Division, Newport.

REFERENCES

1. U. Schumann and K. Krettenaure, Numerical simulation of turbulent convection over wavy terrain, *J. Fluid Mech.* **237**, 261 (1992).
2. T. S. Lund and P. Moin, Large-eddy simulation of a boundary layer on a concave surface, in *10th Symposium on Turbulent Shear Flows, Pennsylvania State University, University Park, PA, August 14–16, 1995.*

3. Breuer and W. Rodi, Large-eddy simulation of turbulent flow through a straight square duct and a 180 degree bend, in *Direct and Large-Eddy Simulation I*, edited by Voke, Kleiser, and Chollet (Kluwer Academic, New York, 1994), p. 273.
4. P. Beaudan and P. Moin, *Numerical Experiments on the Flow Past a Circular Cylinder at Sub-Critical Reynolds Number*, Report No. TF-62, Stanford, University, Stanford, CA, 1994.
5. M. Vinokur, Conservative form of gas dynamic equations, *Recherche Aerospatiale*, **1**, 65 (1974).
6. A. Leonard, Energy cascade in large-eddy simulations of turbulent fluid flows, *Adv. Geophys.* **18**a, 237 (1974).
7. J. F. Thompson, Z. U. A. Warsi, and C. W. Mastin, *Numerical Grid Generation* (Elsevier Science, New York, 1985).
8. M. Vinokur, On one-dimensional stretching functions for finite-differences calculations *J. Comput. Phys.* **50**, 215 (1983).
9. K. Moin and J. Kim, Numerical investigation of turbulent channel flow, *J. Fluid Mech.* **18**, 341 (1982).
10. S. Ghosal and P. Moin, The basic equations for the large eddy simulation of turbulent flow in complex geometry, *J. Comput. Phys.* **118**, 24 (1995).
11. U. Schumann, Subgrid scale model for finite difference simulation of turbulent flows in plane channel and annuli, *J. Comput. Phys.* **18**, 376 (1975).
12. R. Shapiro, Smoothing, filtering, and boundary effects, *Rev. Geophys. Space Phys.* **8**(2), 359 (1970).
13. T. Wei and C. R. Smith, Secondary vortices in the wake of circular cylinders, *J. Fluid Mech.* **169**, 513 (1986).
14. A. Roshko, *On the Drag and Shedding Frequency of Two-Dimensional Bluff Bodies*, NACA Report No. 1191 (1954).
15. S. A. Jordan and S. A. Ragab, An efficient fractional-step technique for unsteady three-dimensional flows, *J. Comput. Phys.* **127**, 218 (1996).
16. M. M. Rai and P. Moin, AIAA 89-0369 (1989).
17. S. K. Lele, Compact finite difference schemes with spectral-like resolution, *J. Comput. Phys.* **103**, 16 (1992).
18. H. Mansy, P. Yang, and D. R. Williams, Quantitative measurements of three-dimensional structures in the wake of a circular cylinder, *J. Fluid Mech.* **270**, 277 (1990).
19. L. L. Pauley, P. Moin, and W. C. Reynolds, The structure of two-dimensional separation, *J. Fluid Mech.* **220**, 397 (1990).
20. C. Norberg, Pressure forces on a circular cylinder in cross flow, in *IUTAM Symposium on Bluff-Body Wakes, Dynamics and Instabilities*, edited by Eckelmann *et al.* (Springer-Verlag, New York/Berlin, 1992), p. 275.
21. W. C. Reynolds, The potential and limitations of direct and large-eddy simulations, in *Whither Turbulence*, edited by J. L. Lumley (Springer-Verlag, New York, 1991).
22. L. Ong and J. Wallace, The velocity field of the turbulence very near the wake of a circular cylinder, *Exper. in Fluids* **40**, 441 (1996).
23. S. Liu, C. Meneveau, and J. Katz, On the properties of similarity models as deduced from measurements in a turbulent jet, *J. Fluid Mech.* **275**, 83 (1994).
24. J. A. Murry, U. Piomelli, and J. M. Wallace, Spatial and temporal filtering of experimental data for a-priori studies of subgrid-scale stresses, *Phys. Fluids* **8**(7), 1978 (1996).
25. U. Piomelli, P. Moin, and J. H. Ferziger, Model consistency in large-eddy simulations of turbulent channel flows, *Phys. Fluids* **31**(7), 1884 (1988).
26. S. Ghosal, Analysis of discretization errors in LES, *Annual Research Briefs*, Center of Turbulent Research, Stanford University, Stanford, CA, 1995.